

## Article

# Climate and Sea Level Controls on the Spatial Heterogeneity of Mid-Holocene Vegetation in the North China Plain

Mingxia Xie<sup>1,2</sup>, Qinmian Xu<sup>3,4,\*</sup>, Yuecong Li<sup>1,2</sup>, Tianyu Du<sup>1,2</sup>, Baoshuo Fan<sup>1,2</sup>, Wensheng Zhang<sup>5</sup> and Bing Li<sup>1,2,\*</sup>

<sup>1</sup> College of Geographical Sciences, Hebei Normal University, Shijiazhuang 050024, China

<sup>2</sup> Key Laboratory of Environmental Evolution and Ecological Restoration of Hebei Province, Hebei Normal University, Shijiazhuang 050024, China

<sup>3</sup> Tianjin Center, China Geological Survey, Tianjin 300170, China

<sup>4</sup> State Key Laboratory of Loess and Quaternary Geology, Institute of Earth Environment, CAS, Xi'an 710061, China

<sup>5</sup> College of Earth and Environmental Sciences, Lanzhou University, Lanzhou 730000, China

\* Correspondence: xqinmian@mail.cgs.gov.cn (Q.X.); 17733838911@163.com (B.L.)

**Abstract:** Understanding the response of regional vegetation succession to climate changes and human activities in the Middle Holocene can help predict the trajectory of future vegetation changes. The North China Plain, modulated by the East Asian monsoon, is sensitive to global climate changes. However, its vegetation type and distribution during the Middle Holocene are still unclear. Based on the comprehensive analysis of 155 samples for pollen and grain sizes as well as other environmental proxies from the LD03 drill core, vegetation was reconstructed quantitatively using the REVEALS model during the period of 8.4–5.5 cal ka BP. (1) Compared to the pollen percentage, the coverage of *Pinus* (13.5%) decreased most significantly, while the coverage of *Quercus* increased significantly (51.3%). The proportion of *Ephedra* (11.9%) increased. A large area of temperate deciduous broad-leaved forests mainly with deciduous *Quercus* developed in the eastern coastal plain of Hebei from 8.0 ka BP to 5.5 ka BP. (2) During 7.4–7.1 ka BP, the proportion of broadleaved trees decreased significantly, while herbaceous plants such as Chenopodiaceae and Poaceae increased. Vegetation components such as *Quercus* and *Pinus* and Chenopodiaceae and Poaceae were sensitive to marine transgression. (3) The vegetation distribution during the Middle Holocene in the eastern and western regions of Hebei was mainly as follows: There was a large area of *Pinus* in the Taihang Mountains in western Hebei, whereas grasslands mainly composed of Asteraceae and Poaceae (*reeds*) developed in the floodplain of central Hebei. Coniferous and broad-leaved mixed forests or temperate deciduous broad-leaved forests developed in the eastern coastal plain of Hebei. The possible mechanisms of vegetation heterogeneity are sea level rise and the enhanced monsoon precipitation.

**Keywords:** pollen; Middle Holocene; quantitative reconstruction of paleo-vegetation



**Citation:** Xie, M.; Xu, Q.; Li, Y.; Du, T.; Fan, B.; Zhang, W.; Li, B. Climate and Sea Level Controls on the Spatial Heterogeneity of Mid-Holocene Vegetation in the North China Plain. *Land* **2022**, *11*, 2051. <https://doi.org/10.3390/land11112051>

Academic Editors: Minmin Ma, Xianyong Cao and Guanghui Dong

Received: 14 October 2022

Accepted: 11 November 2022

Published: 16 November 2022

**Publisher's Note:** MDPI stays neutral with regard to jurisdictional claims in published maps and institutional affiliations.



**Copyright:** © 2022 by the authors. Licensee MDPI, Basel, Switzerland. This article is an open access article distributed under the terms and conditions of the Creative Commons Attribution (CC BY) license (<https://creativecommons.org/licenses/by/4.0/>).

## 1. Introduction

As an important component of terrestrial ecosystem, vegetation is sensitive to climate changes and human activities, and vegetation change may also affect the regional and global environment [1,2]. Vegetation reconstruction is an important means to understand past ecological and global changes and optimize parameters for paleo-climate simulations [3,4]. The warm and humid climate of the Northern Hemisphere during the Middle Holocene could serve as an analogue for the future [5–7], not only for being the most recent warm period to the present, but also for the intensification of human activities. As an indispensable proxy for restoring and simulating paleo-vegetation, pollen are of great significance for quantitative paleo-vegetation reconstructions [8]. There are many quantitative methods for

vegetation reconstructions, such as Biomization [9,10], MAT (Modern Analogy Method) [11–13] and the Landscape Reconstruction Algorithm (LRA) [14]. The LRA algorithm (including the REVEALS and LOVE models) is an important method to quantitatively estimate vegetation coverage and abundance of individual species, which has been widely used in Europe, North America and Africa [13,15,16], Tibetan Plateau [17,18] and North China [19].

The North China Plain, the second largest floodplain in China [20], is located in a humid and semi-humid region and on the west of the Bohai Sea. Studies have shown that coastal lakes and wetlands have formed along the western shore of the Bohai Sea since 9.0 ka BP. The area is sensitive to global changes and sea level rise [21]. The East Asian monsoon has a profound impact on the annual variability of precipitation and vegetation pattern in the North China Plain [22–25]. However, there are still some debates about the vegetation types of the Middle Holocene. Some researchers believed that a temperate deciduous broad-leaved forest had formed [26–33]. The pollen assemblage of the Middle Holocene in the North China Plain showed a high content of broad-leaved tree species, a large variety of herbaceous plants and abundant aquatic plants [26,28]. Other studies have shown that mixed coniferous and broad-leaved forest-steppe vegetation had developed on the plain [34–37]. Studies at Baiyangdian and Handan have shown that mixed coniferous and broad-leaved forests dominated by *Pinus* developed during the Middle Holocene [34,35]. There are several reasons for the controversy. Firstly, there are only a few high-resolution palynological records during the Middle Holocene, especially from the eastern coastal region. Secondly, pollen percentages have always been interpreted as vegetation percentages in previous studies, which ignores the non-linear relationship between pollen and vegetation. In addition, the relationship between vegetation and sea level change during the middle Holocene has rarely been discussed in previous studies.

Here, we carry out pollen, stomatal apparatus, and grain-size analyses based on the LD03 drill core, and reconstruct vegetation in eastern North China plain during 8.4–5.5 cal ka BP through calculating relative pollen production (RPP) using the REVEALS model [14,38]. Stomatal apparatus can be identified to the level of genus with local deposition and developmental characteristics. Based on the reconstruction of vegetation succession process in eastern North China Plain during 8.4–5.5 cal ka BP and synthesis of previous research, we attempt to understand the vegetation pattern and its mechanism, which in turn may provide a scientific basis for ecological restoration in Northern China in the face of global warming and sea level changes.

## 2. Geography of Sampling Site

The sampling site (LD03, 39°06′10″ N, 116°40′57″ E, 9 m asl) is located in the eastern North China Plain with a low and flat terrain (Figure 1). Controlled by the East Asian monsoon, the climate in this area exhibits a marked seasonality. Annual mean temperature is approximately 11.5 °C. Annual precipitation is 543.6 mm, mostly occurring in summer with great interannual variations. The natural vegetation has been seriously cleared. At present, crops such as *Triticum aestivum*, *Setaria italica*, *Zea mays* L., *Arachis hypogaea* L., and so on are cultivated in the region along with fruit trees, such as *Prunus persica*, *Prunus armeniaca* L., and *Populus* L.

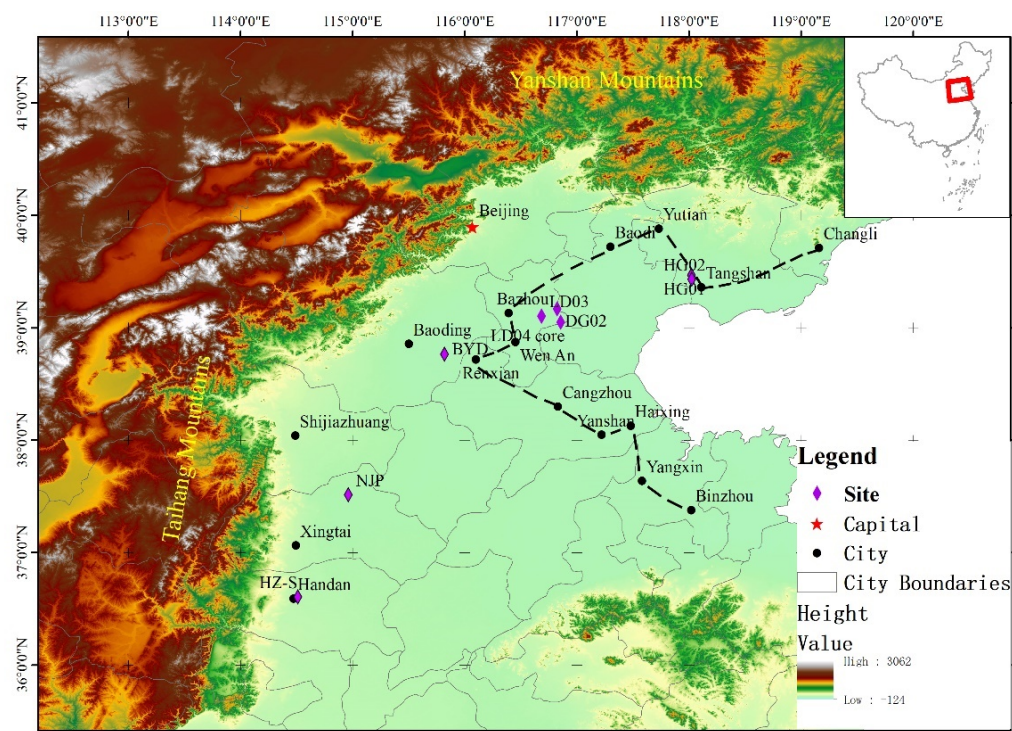


**Figure 1.** Geographical location of the study area and location of sampling sites. - - - - : Middle Holocene Bohai Bay maximum marine transgression boundary; ◆ : LD03, LD04 and DG02 are three parallel drill cores; HG01, HG02, BYD, NJP and HZ-S are comparative cores and profiles for studying vegetation patterns.

### 3. Materials and Methods

#### 3.1. Regional Stratigraphic Investigation

Considering that the study area is the largest range of marine transgression in the Middle Holocene, we have carried out stratigraphic investigations at spatial intervals of 10–20 km. Three cores (named hereafter as LD03, DG02 and LD04) were selected to represent the lithology and chronology of the regional strata (Figure 1 and Table A1). Sediments from 708–1445 cm of the LD03 core (80 m long) were selected for this study. This section can be divided into nine sedimentary units. Sediments from 0–1000 cm of the LD04 core (39°02′57″ N, 116°51′14″ E, 4 m asl, 71 m long), located at 10 km southeast of the LD03 core, were also selected for this study. This section can be divided into eight sedimentary units. The DG02 core (39°10′04″ N, 116°49′27″ E, 4 m asl, 30 m long) is located approximately 12 km northeast of the LD03 core. Please see the lithologic descriptions and photographs in Appendix A.

#### 3.2. Sediment Dating

Organic sediments and plant materials at a depth of 537 cm, 786 cm and 875 cm in LD03 core, 1150 cm in DG02 core and 910 cm in LD04 core were selected for AMS  $^{14}\text{C}$  dating. The dating samples were test in Xi'an Accelerator Mass Spectrometry Center, institute of Earth Environment, Chinese Academy of Sciences and Beta laboratory.

### 3.3. Grain-Size Analyses and End-Member Modeling

The aim of End-Member Analysis (EMMA) is to obtain the distinct dynamic components of the whole sediment core. End-members represent a set of fixed combinations that can be viewed as different subsets of the granular datasets in the study area [39]. EMMA can distinguish different grain-size components to identify the source and dynamic conditions of sediments, which has been widely used in various sedimentary environments [40–43]. In this study, the model was run in the R software environment [44,45].

### 3.4. Pollen Analyses and Quantitative Vegetation Reconstruction

Sediments at 775–1326 cm depths from the LD03 core were mainly composed of grey and dark-grey silty clay and sandy silt, indicating a coastal wetland and swamp environment, which appear to yield enough pollen for paleo-vegetation reconstruction. A total of 155 samples were selected for pollen analysis with sampling intervals of 1–2 cm. Pollen extraction was carried out by the conventional HCl–NaOH–HF method [46] and the heavy liquid flotation method. More than 400 pollen grains were counted for each sample. The sediment samples for grain-size analysis were pretreated according to conventional methods [47,48] to remove impurities such as organic matter and calcium carbonate. The identification and particle-size analysis of pollen grains and stomata were completed in the Environmental Evolution Laboratory of the School of Geographical Sciences, Hebei Normal University.

The computer program REVEALS v6.2.2 [14] is used to reconstruct paleo-vegetation. The input data are relative pollen production (RPP), pollen sedimentation rate, fossil pollen data and its variance–covariance matrix. A total of 10 common genera including *Pinus*, *Quercus*, *Betula* and others were selected for quantitative reconstruction. The RPP of *Quercus*, *Pinus*, *Asteraceae*, *Artemisia* and *Chenopodiaceae* in the Yanshan Mountains and the RPP of *Betula*, *Ulmus*, *Carpinus*, *Ephedra* and *Urtica* + *Humulus* in the temperate deciduous broad-leaved forests of northern China were used in this work (Table 1) [38,49]. The paleo-vegetation was reconstructed with *Quercus* as a reference species.

**Table 1.** Pollen productivity and productivity integration for various taxa [39,50].

Taxa	Sedimentation Rate (m/s)	Relative Pollen Production
<i>Pinus</i>	0.0247	15.81 ± 1.94
<i>Quercus</i>	0.0216	1.0
<i>Betula</i>	0.012	3.08 ± 0.01
<i>Ulmus</i>	0.021	1.643 ± 0.02
<i>Carpinus</i>	0.024	1.539 ± 0.02
<i>Ephedraceae</i>	0.015	0.195 ± 0.02
<i>Asteraceae</i>	0.0084	3.69 ± 0.2
<i>Artemisia</i>	0.011	7.1 ± 0.3
<i>Chenopodiaceae</i>	0.0134	9.5 ± 0.5
<i>Urtica</i> + <i>Humulus</i>	0.01	3.335 ± 0.01

In order to better understand the vegetation characteristics of North China Plain during the Middle Holocene, we digitized the pollen assemblage of four previously studied sites, and then input into the REVEALS model for vegetation reconstruction (Figure 2). Pollen data are from the Longhu HZ-S core in Handan city [36], the Dacaozhuang profile in Xingtai city (unpublished data), Anxin section in Baoding city [50] and the Caofeidian core in Tangshan city (HG01 and HG02) [51] (Figure 1). For the relative pollen production (RPP) for pollen data reanalysis, we refer to Sun et al. (2022) [52].

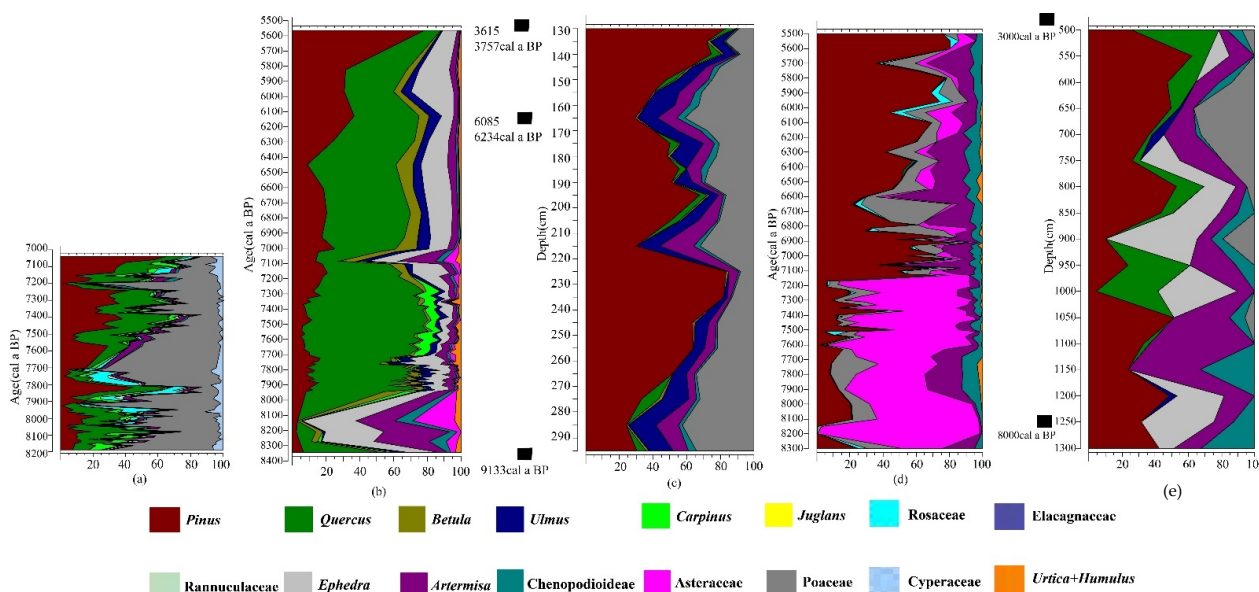


**Figure 2.** Comparison of vegetation reconstruction at different sites in Hebei ((a) Caofeidian, (b) Shengfang LD03 core, (c) Baiyangdian, (d) Ningjinpo and (e) Handan Longhu Park).

### 3.5. Chronological Framework of the LD03 Core

In order to establish an accurate age framework, we describe the lithology and dating of the LD03 (a depth of 1326–775 cm) (Figure 3) and other parallel cores (Table A1 and Figure A1). Sedimentary unit 3–IX in LD03 is mainly peat and organic clay, and the basal age is 5653–5490 cal a BP. The sedimentary units 2–III in DG02 core, 3–V in LD03 and 4–IV in LD04 core are all interbed bed dark-gray silty sand and silty clay. The underlying sedimentary units 2–II in DG02, 3–IV in LD03 core and 4–III in LD04 are horizontally bedded; the <sup>14</sup>C age of 2–II in DG02 core is 7982–7916 cal a BP, and the <sup>14</sup>C age of the underlying sedimentary unit 4–II in LD04 core are 8337–8188 cal a BP. Therefore, the age of 3–IV in LD03 core is estimated to 8260–7950 cal a BP, and the sedimentary unit 3–III is composed of Early-Holocene sediments. The difference of organic carbon reservoir age and <sup>14</sup>C age of plant remains in this region is less than 100 years (a decade or decades) [53,54]. The age–depth was established using ages from the DG02, LD03, and LD04 cores (Figure 3), and the organic carbon reservoir effect was corrected [55]. As can be seen from Appendix A, the regional stratum is spatially continuous, and the ages of the same strata can refer to each other. Thus, one sample is from the DG02 core, three samples from the LD03 core and one sample from the LD04 core, which were collected for <sup>14</sup>C dating (Table 2). All the dating materials were plant remains and organic clay. The IntCal20 database was used for age calibration, and the age–depth model was established using Bacon in R software [56] (Figure 4).

**Table 2.** AMS <sup>14</sup>C ages of cores DG02, LD03 and LD04.

Borehole No.	Lab ID	Depth (cm)	Materials Dated	Radiocarbon Age (a BP)	Calibrated Age (cal a BP)	Median-Probability Age (cal a BP)	δ <sup>13</sup> C (‰, PDB)
DG02	Beta-556146	1105	Plant remains	7100 ± 30	7982–7916	7949	−28.3
LD03	Beta-563687	537	Organic sediment	3500 ± 30	3855–3692	3774	−23.1
LD03	XA53772	786	Organic sediment	4865 ± 20	5653–5490	5572	−27.9
LD03	XA53773	875	Organic sediment	6075 ± 25	7149–6803	6976	−25.7
LD04	XA53774	910	Organic sediment	7440 ± 25	8337–8188	8263	−30.3

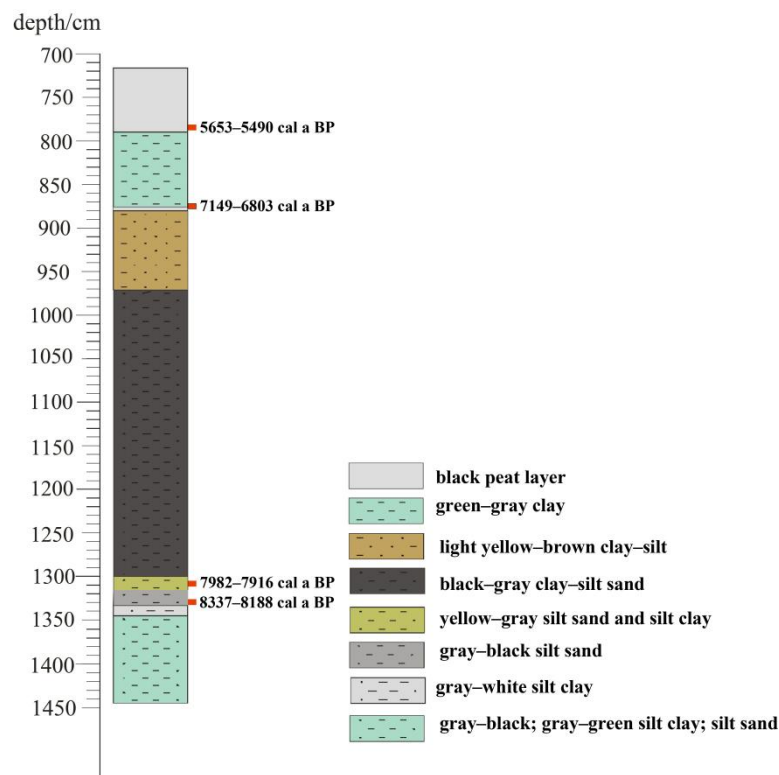


Figure 3. LD03 core lithology map.

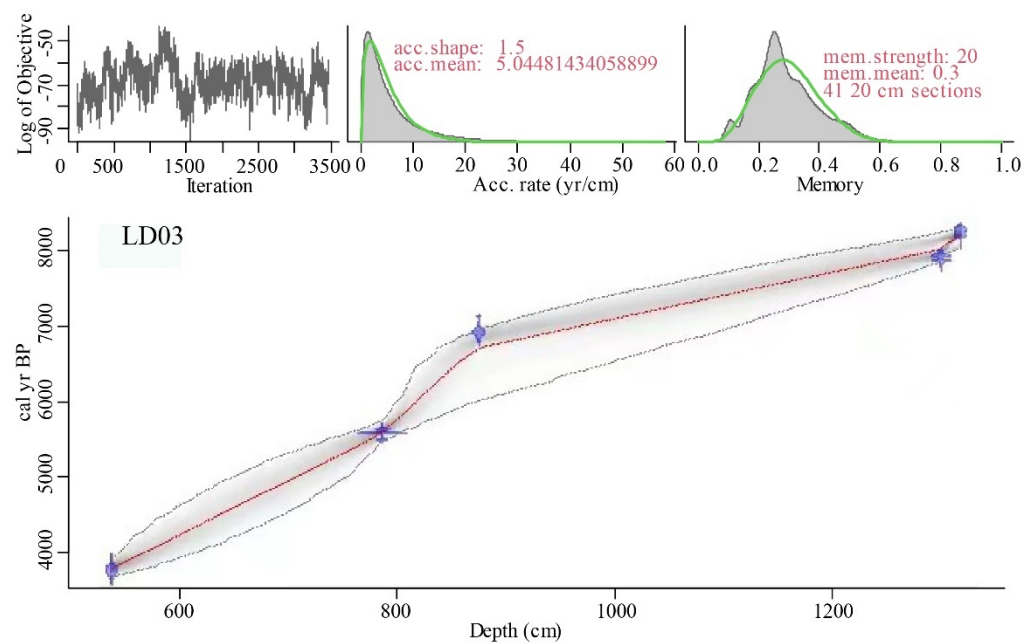


Figure 4. Age–depth model of the LD03 core.

## 4. Results

### 4.1. Pollen Assemblage and Stomata Concentration

A total of 68 pollen types were identified in 155 pollen samples, including 14 species of trees, 9 species of shrubs, 29 species of herbs, 12 species of ferns and 4 species of algae. Common tree pollen types include *Pinus*, *Quercus*, *Betula*, *Ulmus*, *Carpinus* and *Picea* sporadically; shrub pollen types include Rosaceae, *Hippophae*, *Ephedra*, Elaeagnaceae and *Corylus*; herb pollen types include *Artemisia*, Chenopodiaceae, Poaceae (reeds < 30 μm),

Asteraceae, Cyperaceae, *Urtica* + *Humulus* and a small quantity of Brassicaceae; aquatic pollen include *Myriophyllum*, *Typha* and Potamogetonaceae; ferns are mainly *Selaginella sinensis*, Polypodiaceae, Gleicheniaceae, *Monoletes*, *Triletes*, *Selaginella* and *Ceratopteris*, which account for a small quantity; common algae are *Pediastrum* and *Spiniferites*. The percentage of terrestrial pollen is calculated based on the total number of identified pollen of all terrestrial taxa, and the percentage of aquatic pollen is calculated on the basis of the total number of all aquatic plants. According to the pollen assemblage characteristics changes, the pollen percentage data were clustered using CONISS analysis and divided into four pollen zones and five subzones (Figure 5).

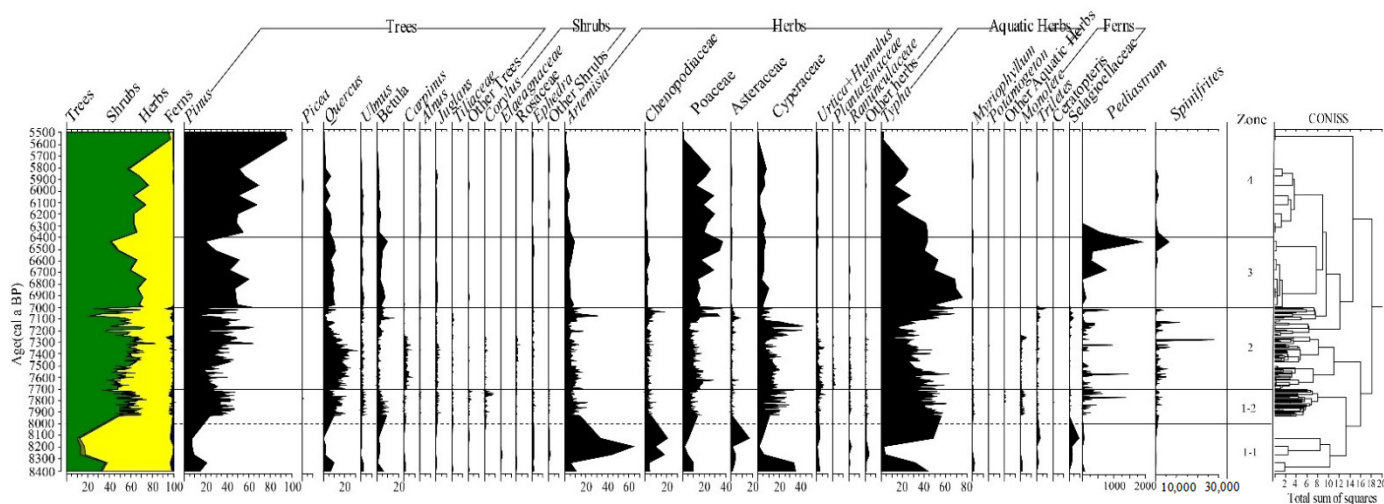


Figure 5. Diagram of pollen percentage of the LD03 core.

Zone 1 (1326–1229 cm, 8.4–7.7 cal ka BP): The relative abundance of tree pollen (53.1%) is high, including *Pinus* (32.5%), *Quercus* (11.7%), *Betula* (4.6%), *Ulmus* (1.8%) and *Juglans* (1.0%). The pollen percentage of shrubs was averaged at 1.8%. The average pollen percentage of terrestrial herbs was 43.3%, with Cyperaceae (14.6%) as the dominant taxa, followed by *Artemisia* (11.4%), Poaceae (reeds < 30  $\mu\text{m}$ , 8.7%), Chenopodiaceae (4.1%), *Urtica* + *Humulus* (1.6%) and Asteraceae (1.3%). The average pollen percentage of aquatic herbs was 41.9%, and *Typha* (41.2%) was the main component. The ferns' spore percentage was 1.7%. The concentration of *Pediastrum* is 51 grains/g, and the concentration of *Spiniferites* is 417 grains/g. During the period of 7920–7700 cal a BP, the stomata concentration of Cupressaceae was 9 grains/g and the stomata concentration of *Pinus* was 2 grains/g (Figure 6). This zone can be divided into two subzones.

Subzone 1–1 (1326–1310 cm, 8.4–8.0 cal ka BP): The pollen percentage of terrestrial herbs was relatively high, with an average of approximately 74.7%, and *Artemisia* (31.4%) represents the main component; tree pollen (21.2%) and aquatic herbs (*Typha*, 25.9%) were at the lowest value during the study period.

Subzone 1–2 (1300–1229 cm, 8.0–7.7 cal ka BP): The tree pollen percentage (57.6%) increased. *Pinus* (35.3%) was the main component. Terrestrial herbs pollen (38.9%) was dominated by *Artemisia* (8.6%) and Chenopodiaceae (3.1%). Aquatic herbs were dominated by *Typha* (43.3%). The concentrations of *Pediastrum* (55 grains/g) and *Spiniferites* (467 grains/g) increased compared with Subzone 1–1.

Zone 2 (1127–885 cm, 7.7–7.0 cal ka BP): The tree (54.7%) and terrestrial herb pollen percentage (42.4%) changed slightly compared with Zone 1. Tree pollen was dominated by *Pinus* (33.7%) and *Quercus* (13.9%), and herbs pollen was mainly Poaceae (reeds < 30  $\mu\text{m}$ , 12.7%) and *Artemisia* (7.9%). The concentration of *Pediastrum* increased to 92 grains/g, and *Spiniferites* concentration culminated (1487 grains/g).

Zone 3 (880–840 cm, 7.0–6.4 cal ka BP): Tree pollen percentage (62.6%) in this zone was higher than that of Zone 2, with *Pinus* (45.3%) and *Quercus* (8.8%) increasing. Terrestrial

herbs (36.6%) declined. Aquatic herb pollen percentage (56.1%) was obviously higher than that of Zone 2, with an obvious increase of *Typha* (56.0%). The concentration of *Pediastrum* increased to the highest value of 382 grains/g and the concentration of *Spiniferites* significantly reduced to 820 grains/g.

Zone 4 (835–775 cm, 6.4–5.5 cal ka BP): Tree pollen percentage (72.0%) increased compared with Zone 3, specifically *Pinus* (64.0%). The pollen percentage of terrestrial herbs (27.1%) decreased slightly. The concentration of *Pediastrum* was 58 grains/g, and the *Spiniferites* concentration (445 grains/g) decreased continuously.

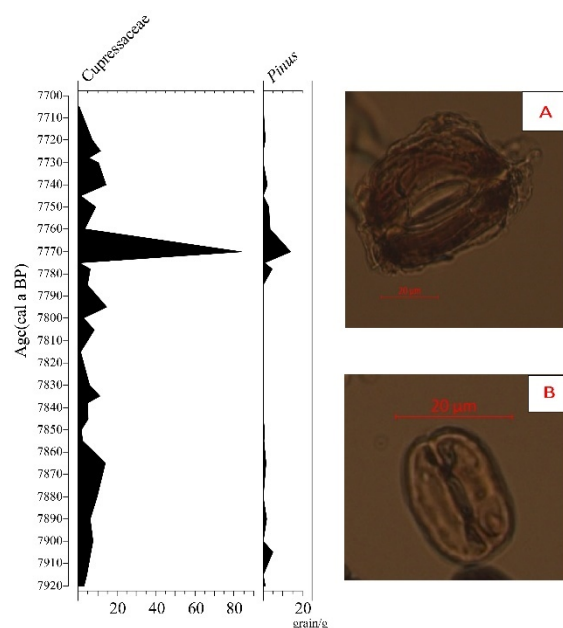


**Figure 6.** Stomata concentration of the LD03 core. Image (A) is *Pinus* and (B) is Cupressaceae.

#### 4.2. Quantitative Reconstruction of Paleo-Vegetation

The total average pollen content of these 10 genera in the core was more than 90%. At present, there are no data on relative pollen production of Cyperaceae, Poaceae (*reed*) and *Typha* in China, so we did not reconstruct wetland plants. The reconstruction results show that the cover of tree plants decreased compared to pollen percentage, and the cover of *Pinus* decreased most significantly, accounting for approximately 13.5% (2.7–78.2%). The overall percentage of herb pollen also decreased, such as *Artemisia* with 5.0% (1.3–35.7%) and the decrease of herb coverage was more obvious than their pollen percentages. The proportions of the different plant types varied in the rest of the period. According to the reconstruction results, the vegetation succession can be divided into five zones (Figure 7).

8.4–8.0 cal ka BP (Pollen Subzone 1–1). The total coverage of trees (28.0%) was the lowest during the study period, among which *Quercus* accounted for the highest percentage at 15.9%, followed by *Pinus* (4.1%), *Betula* (3.7%), *Ulmus* (2.3%) and *Carpinus* (1.9%). Shrubs was mainly *Ephedra*, which covered 28.7%. The coverage of upland herbs was approximately 43.3%, which was the highest value during the study period, mainly consisting of *Artemisia* (25.1%), followed by Asteraceae (9.0%), Chenopodiaceae (6.8%) and *Urtica* + *Humulus* (2.4%). Thus, semi-arid grasslands dominated by *Artemisia*, Asteraceae and *Ephedra* developed during this period.

8.0–7.7 cal ka BP (Pollen Subzone 1–2). The total coverage of trees was 78.1%, which is much higher than that of the previous zone, and *Quercus* cover (53.1%) increased obviously followed by *Pinus* (11.9%). *Ephedra* (13.0%) decreased significantly; herbaceous plants (9.0%) obviously decreased compared with Zone 1–1; *Artemisia* (4.5%) was the most common upland herb. The vegetation in the area was a mixed coniferous and broad-leaved forest dominated by *Pinus* and *Quercus*.

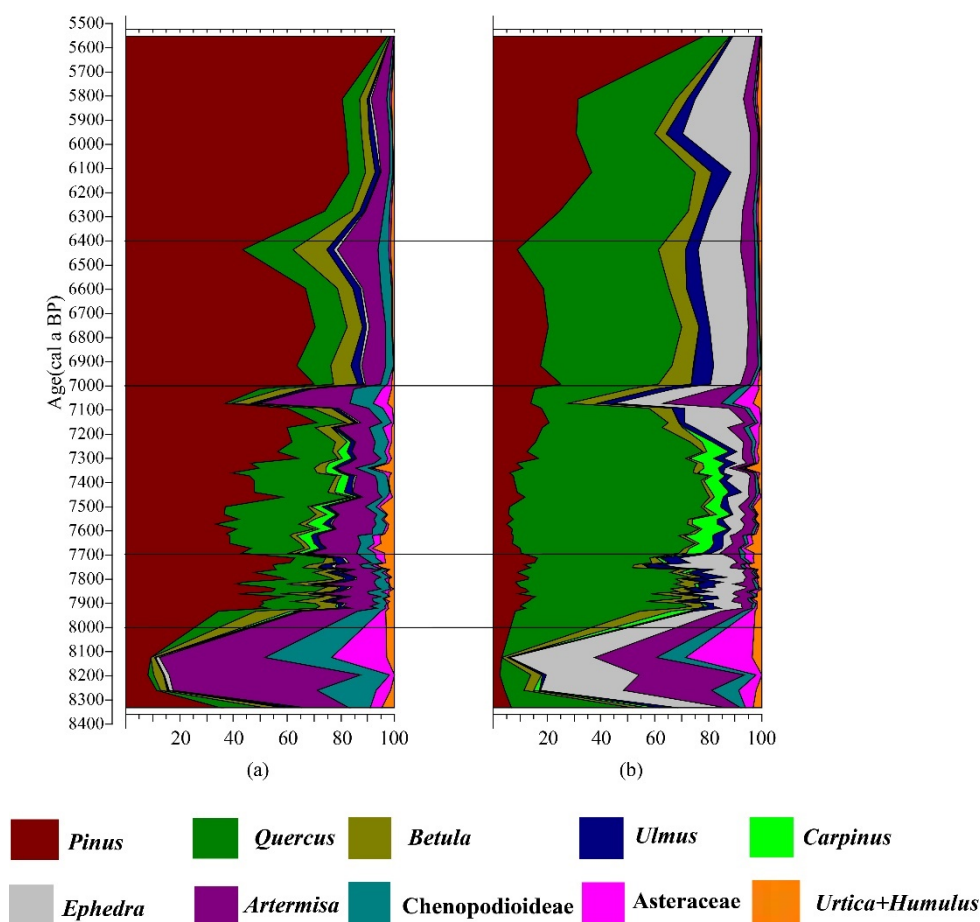


**Figure 7.** Percentage of pollen (a) and vegetation (b) based on LRA reconstruction in the LD03 core.

7.7–7.0 cal ka BP (Pollen Zone 2). The tree coverage (82.7%) increased to the highest value among all zones, dominated by *Quercus* (60.0%) and *Pinus* (10.6%); herbaceous plants (9.9%) had no significant changes compared with the previous stage. The vegetation in the area was temperate deciduous broad-leaved forest dominated by *Quercus* or mixed coniferous and broad-leaved forest dominated by *Pinus* and *Quercus*.

7.0–6.4 cal ka BP (Pollen Zone 3). The coverage of trees (79.4%) was slightly lower than that of Zone 2, mainly including *Quercus* (46.9%) and *Pinus* (18.0%); herbaceous plants (6.5%) decreased compared with Zone 2. Among these, the coverage of *Artemisia* (3.9%) declined. The vegetation in the area was a mixed coniferous and broad-leaved forest dominated by *Pinus* and *Quercus*.

6.4–5.5 cal ka BP (Pollen Zone 4). The vegetation coverage of trees (80.8%) increased slightly, and *Pinus* (40.4%) increased significantly. The proportion of herbaceous plants (5.0%) decreased to the lowest value during the period, dominated by *Artemisia*, which declined to 2.9%. The vegetation in the area was a mixed coniferous and broad-leaved forest dominated by *Pinus* and *Quercus*.

#### 4.3. End-Member Analysis

The results of grain-size EMMA analysis show that the samples can be decomposed into three end-members (EM1, EM2 and EM3), which explained 65% and 88% of class-wise and sample-wise variances, respectively, with high degrees of reliability. EM1 is a unimodal curve with a mode of approximately 7.2  $\phi$  (6.8  $\mu\text{m}$ ). The sediment particle size is relatively small, the frequency curve has a low and wide peak and the sorting is poor, indicating that EM1 represents a palustrine or lacustrine environment [57]; EM2 has a double peak, the mode of the main peak is 4.8  $\phi$  (35.9  $\mu\text{m}$ ), and the mode of the secondary peak is 0.9  $\phi$  (1918.5  $\mu\text{m}$ ). The source may be proximal surface runoff. EM3 belongs to the end-member

of medium and fine sand. The frequency curve has nearly normal distribution. The kurtosis is sharper and the sorting is better, indicating strong sedimentary dynamic conditions. The sediments may come from marine environments. The sediments in the LD03 core are dominated by EM1 and EM3. The EM1 component accounted for 43% of the total visual variance, EM2 accounted for 11% of the total visual variance, and EM3 accounted for 47% of the total visual variance. The results of EMMA can be used to define five zones of grain-size variations (Figure 8).

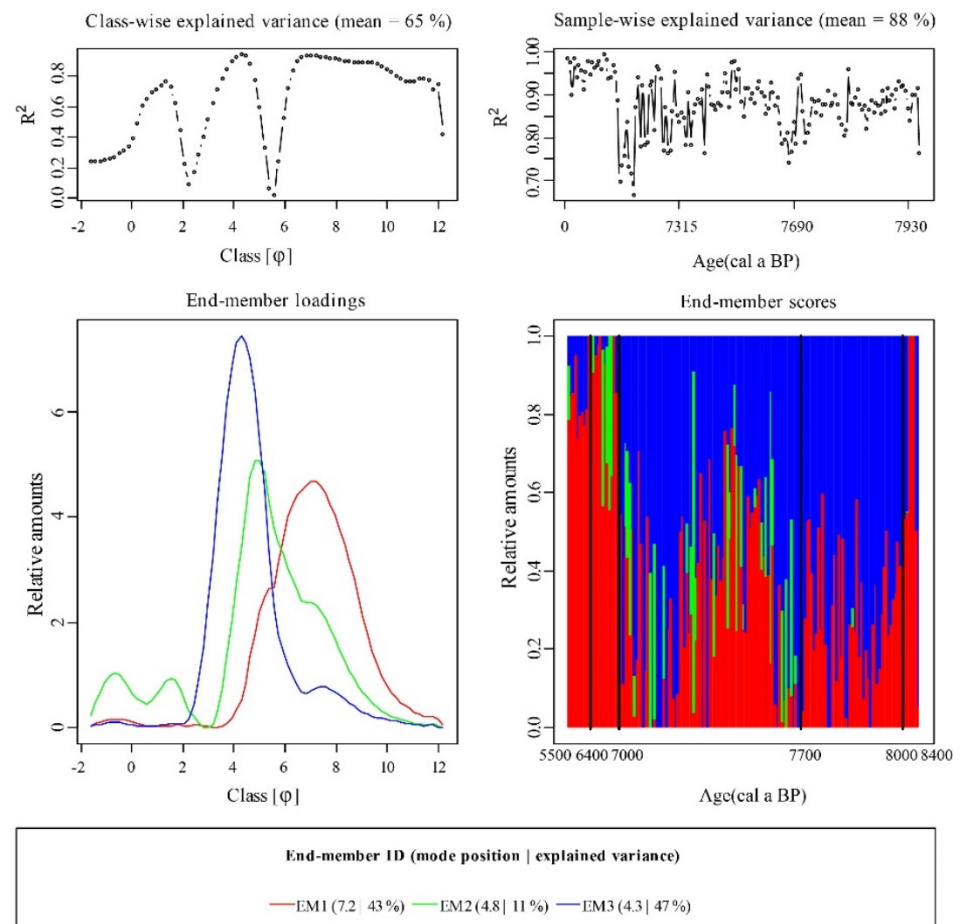


**Figure 8.** Particle size end-member composition of the LD03 drill core.

**Zone 1** (1326–1310 cm, 8.4–8.0 cal ka BP): This zone is dominated by EM1 (71.1%) with finer grain size; the average content of EM3 is 28.9%.

**Zone 2** (1310–1229 cm, 8.0–7.7 cal ka BP): This zone is mainly composed of EM3 (72.5%) with a coarser grain size, which is much higher than that of Zone 1; EM1 accounts for 27.3%.

**Zone 3** (1129–885 cm, 7.7–7.0 cal ka BP): This zone is mainly composed of EM3 (57.2%) with a coarser particle size, which is much lower than that of Zone 2; EM1 (32.6%) and EM2 (10.2%) increased slightly.

**Zone 4** (880–845 cm, 7.0–6.4 cal ka BP): This zone is mainly composed of EM1 (83.2%) with finer particle size, which is significantly higher than in Zone 3; the content of EM3 (3.1%) is significantly lower than that of Zone 3; EM2 (13.8%) shows little change compared with Zone 3.

**Zone 5** (840–775 cm, 6.4–5.5 cal ka BP): This zone is mainly composed of EM1 (83.6%) with finer particle size, which changed slightly compared with Zone 4; the average content of EM3 is 15.0%; EM2 (1.4%) significantly decreased compared with Zone 4.

## 5. Discussion

### 5.1. Depositional Environment during 8.4–5.5 ka BP

Sedimentary environment during 8.4–5.5 ka BP in the study area was divided into three stages based on the changes in grain-size end-members and the concentration of *Spiniferites* and *Pediastrum* (Figure 9).

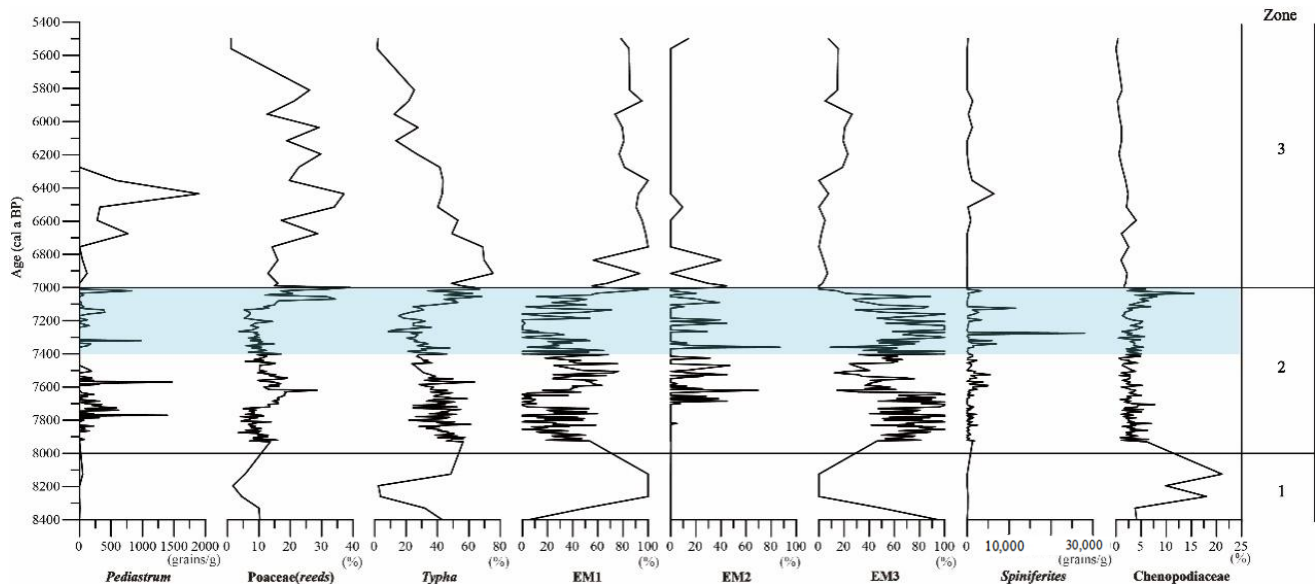


**Figure 9.** Comparison of the concentrations of *Spiniferites* and *Pediastrum*, the percentages of Poaceae (*reeds*), *Typha* and Chenopodiaceae and the grain-size EM scores.

**Zone 1 (8.4–8.0 cal ka BP):** The proportional abundance of EM1 and drought-tolerant herbs (Chenopodiaceae) was high, and the percentage of aquatic plants (*Typha* and Poaceae (*reeds*)) was low, indicating a shallow lacustrine environment and dry climate.

**Zone 2 (8.0–7.0 cal ka BP):** EM3 component increased obviously, and EM1 decreased with fluctuations. The concentration of *Spiniferites*, which lives in a brackish environment of the littoral or shallow marine areas, increased [58–60]. The concentration of *Pediastrum*, *Typha* and Poaceae (*reeds*) decreased significantly. The *Pediastrum* concentration suggests a freshwater environment and freshwater lake levels [61]. All the above shows that salinity increased and sea level rose. During the period of 7.4–7.0 cal ka BP, the concentration of *Spiniferites* culminated, and the EM3 component, which represents the marine source, were more than 80%. Therefore, it was concluded that the Bohai Sea transgression reached the Shengfang area [62]. Previous studies showed that sea level rose rapidly (6.4 mm/a) at 8.5–7.5 cal ka BP, and the coastal line invaded westward land [62]. The Bohai Sea transgression reached the Shengfang area at 7.6–7.1 ka BP [62].

**Zone 3 (7.0–5.5 cal ka BP):** The composition of sediments was dominated by the EM1 component, *Pediastrum* concentration, and the pollen percentages of *Typha* and Poaceae (*reeds*) increased. The EM3 component decreased sharply, and *Spiniferites* concentration gradually decreased until it disappeared. All above showed that coastline retreated, and the study area became a freshwater lake or wetland marsh, and finally evolved into land. Previous studies also showed that the rate of sea level rise decreased to 1.9 mm/a at approximately 7.0 cal ka BP, and the coastline receded [63,64].

### 5.2. Landscape Changes during 8.0–5.5 cal ka BP in the Eastern Hebei Plain

According to the vegetation reconstruction based on the REVEALS model, vegetation changes in the study area during the period of 8.0–5.5 cal ka BP are mainly divided into three stages.

At the stage of 8.0–7.0 cal ka BP, tree coverages accounted for 80.4%, which was significantly higher than the previous stage. The vegetation was mixed coniferous and broad-leaved forest dominated by *Quercus* (56.6%) and *Pinus* (11.2%). Wetland landscapes composed of Cyperaceae, *Typha* and Poaceae (reeds) developed locally. Stomatal organs of *Pinus* and Cupressaceae, which only scattered within 20 m of the stand, were found in this stage [65–68]. It suggests that coniferous forests such as Cupressaceae and *Pinus* forests developed locally in this area. During this time period, the proportion of deciduous trees was the largest, which may be related to the enhanced East Asian Summer Monsoon (EASM), and the increase of regional humidity with the rising sea level [64,69]. Many research results have shown that the EASM was strong in North China during approximately 8.0–5.5 ka BP, with a warm and humid climate and more rainfall [70–73]. The vegetation types were mainly coniferous forests dominated by *Pinus* and broad-leaved forests dominated by deciduous *Quercus*. The tree pollen percentage increased significantly and reached the maximum, while the percentage of herbs decreased.

During the period of 7.4–7.1 cal ka BP (Figure 8), there was a significant decrease in the proportion of broad-leaved trees, which was related to the enlarged Bohai Sea transgression. Sea level rise leads to the increase of coastal groundwater level and salinity, which was detrimental to the survival of broad-leaved trees such as *Quercus*. In the southern coastal area of China, the transgression culminated at approximately 8.5–7 ka BP. Vegetation showed a sharp decrease in broad-leaved tree species, such as evergreen *Quercus* and *Fagus*, an increase in salt-tolerant Chenopodiaceae, a decrease in freshwater algae such as *Pediastrum* and an increase in salt-tolerant algae such as *Spiniferites* [74–76]. The maximal transgressions occurred in the northern coastal area of China around 7.5 ka BP. Vegetation showed a decrease in broad-leaved trees such as deciduous *Quercus* and *Ulmus*, and an increase in herbaceous plants such as *Artemisia*, Chenopodiaceae and Poaceae (such as at HG01 and HG02 cores in Caofeidian) [51]. Some studies also showed a decrease in the percentage of *Quercus* and a sharp increase in the percentage of *Pinus*, and the concentration of *Phyllostachys*, *Polysphaeridium zoharyi* along with sea level rise [58]. All the above showed that the forest especially the broad-leaved tree decreased obviously, and *Pinus* and salt-tolerant herbs such as Chenopodiaceae and Poaceae may increase when the area was transgressed by a sea level rise. Therefore, trees such as evergreen *Quercus* and *Fagus*, deciduous *Quercus* and *Pinus* and the salt-tolerant herbaceous plants are sensitive to regional climate change and marine transgression.

During the period of 7.0–6.4 cal ka BP, the tree coverage increased to 79.4%, and mixed coniferous and broad-leaved forests (primarily *Pinus* and *Quercus*) grew on the coastal plain. Wetlands dominated by *Typha* and Poaceae (reeds < 30 µm, 15.4%) developed locally. During the period of 6.4–5.5 cal ka BP, *Pinus* coverage increased sharply, *Typha* content decreased obviously and algae disappeared. Coniferous and broad-leaved mixed forest landscapes mainly with *Pinus*, *Quercus*, and *Ephedra* developed on the coast.

### 5.3. Re-Understanding the Vegetation Succession Pattern during 8.0–5.5 cal ka BP in Hebei

The vegetation type that developed in the North China Plain in terms of temperate deciduous broad-leaved forest or coniferous broad-leaved mixed forest and grassland has been a long-standing debate. Therefore, we reconstructed the vegetation of the central North China plain based on the HZ-S core in Handan city [35], the Dacaozhuang profile in Xingtai city (unpublished data), Anxin section in Baoding city [50] and the Caofeidian core in Tangshan city (HG01 and HG02) [51] (Figure 1) using the REVEALS model.

The HG01 and HG02 cores from Caofeidian in eastern Hebei province show that trees and shrubs accounted for 30–83%, and *Pinus* and deciduous broad-leaved trees accounted for 5–40% and 25.9%, respectively, during the time period of 7.5–7 cal ka BP. The herbaceous plants coverage was 48.3%. Our work shows that in the time period of 8.0–5.5 cal ka BP, *Pinus* accounted for 8–68% and deciduous broad-leaved trees accounted for 65.6%, among which *Quercus* (50.5%) dominated. Therefore, these results show that temperate deciduous broad-leaved forests or mixed coniferous and broad-leaved forests dominated by *Quercus* and *Pinus* developed in the eastern coastal areas during the Middle Holocene. The Baiyangdian pollen record shows that in the period of 8.5–5.5 cal ka BP, *Pinus* coverage was 30–80%, and deciduous broad-leaved trees including *Ulmus* (9.6%) and *Quercus* (2.2%) accounted for 12.9%. The Dacaozhuang section indicated that *Pinus* coverage was 5–70% during the period of 7.5–5.5 cal ka BP. Especially after 7ka BP, the coverage of *Pinus* was as high as 58.5%, and the deciduous broad-leaved tree coverage was less than 2%. The Longhu HZ-S core in Handan shows that *Pinus* coverage accounted for 5–50%, and deciduous broad-leaved trees, mainly including *Quercus* (11.2%), *Ephedra* (14.3%) and *Ulmus* (2.0%), accounted for 27.6%. The Longhu HZ-S core in Handan, the Dacaozhuang section in Xingtai city and the Baiyangdian section in Baoding city, all located in the alluvial fan of the Taihang Mountains, evolved into big lakes in the Middle Holocene. The pollen grains mainly come from the local vegetation around the lake and the vegetation in the Taihang Mountains [50,77]. Previous studies have shown that the pollen of *Pinus*, *Quercus* and *Carpinus* in southern Hebei Plain topsoil mainly comes from the Taihang Mountains, thereby representing the regional vegetation [78]. Therefore, in the Middle Holocene (7.0–5.5 cal ka BP), the Taihang Mountains and the interior of the North China Plain may have been covered by a large area of *Pinus*, while in the eastern North China Plain, coniferous and broad-leaved mixed forests dominated by *Quercus* or temperate deciduous broad-leaved forests developed in the coastal areas.

Although the central part of the North China Plain belongs to the same climate zone as the coastal plain, there is a significant difference in vegetation type. The reasons for the difference in vegetation among the eastern coastal area, western mountains and hinterland of the plain might be influenced by the strong EASM and sea level rise in the Middle Holocene (Figure 10). During the Middle Holocene, the combined effects of the inward migration of the coastline and climate warming led to increased water vapor supply as well as increasing monsoonal precipitation, which in turn increased humidity in coastal areas and resulted in the formation of large areas of deciduous broad-leaved forest and coniferous broad-leaved mixed forest in the coastal upland and Yanshan Mountains. During 7.4–7.1 cal ka BP, transgression expanded to the study area, broad-leaved forests decreased and increased herbaceous plants with increased soil salinity and altered hydrothermal conditions, although marine transgression in the Middle Holocene reached the study area and was close to Baiyangdian. However, due to the existence of the Cangxian uplift, seawater did not intrude into the plain lakes (e.g., Baiyangdian). Therefore, the vegetation of the interior plains and the coastal wetland was different in the Middle Holocene. Due to the development of meandering flows as well as flooding of rivers and lakes, the increase of soil moisture led to the development of herbs, and possibly large areas of pine forests and scattered broad-leaved forests in the highlands of North China hinterland [51,79,80]. A large area of *Pinus* developed on the eastern Taihang Mountains instead of climax community-temperate deciduous broad-leaved forests, which might be related to the enhanced monsoonal precipitation during the Middle Holocene [81,82]. Although the coastline shifted inland and the monsoonal precipitation increased, humidity was not sufficiently high for the development of deciduous broad-leaved forests on the Taihang Mountains.

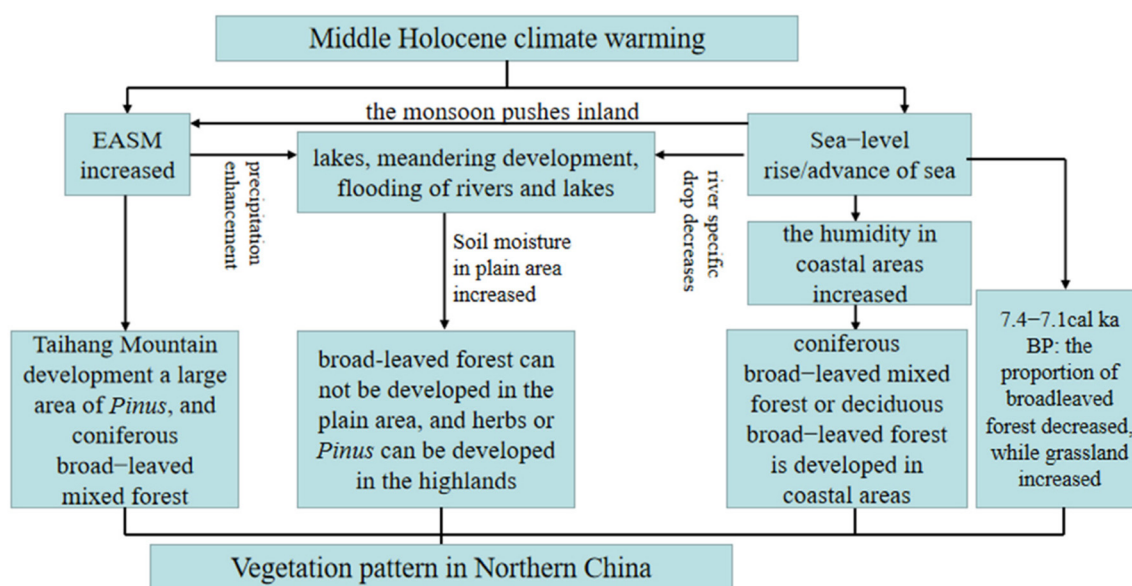


Figure 10. Main mechanism of vegetation pattern formation in North China.

## 6. Conclusions

In order to understand vegetation pattern in the North China Plain during the Middle Holocene and to predict the future trend of vegetation development in coastal areas under the background of climate warming and sea level rise, we analyzed regional environment changes and reconstructed the vegetation quantitatively in the eastern part of the North China Plain using the REVEALS model. The results are as follows:

(1) Compared with pollen percentage, the coverage of trees shows a downward trend. Specifically, the coverage of *Pinus* (13.5%) decreased most significantly, while the coverage of *Quercus* increased significantly (51.3%). The proportion of drought-tolerant *Ephedra* (11.9%) increased.

(2) During 7.4–7.1 ka BP, the proportion of broad-leaved trees decreased significantly on the eastern coast of North China, salt-tolerant herbs such as Chenopodiaceae and Poaceae (*reeds*) and *Spiniferites* concentration increased and freshwater algal concentrations decreased, due to the maximal westward marine transgression of the Bohai Sea. Through a comprehensive synthesis of vegetation changes in the coastal areas in North China, we found that the vegetation components of deciduous *Quercus*, evergreen *Quercus*, *Pinus*, *Chenopodium* and Poaceae, are sensitive to sea level rise during the Middle Holocene.

(3) The vegetation pattern of the North China Plain exhibits a remarkable spatial heterogeneity during the Middle Holocene. There was a large area of *Pinus* in the Taihang Mountains to the west, and grasslands mainly composed of Asteraceae and Poaceae (*reeds*) developed in the hinterland of the North China Plain, whereas coniferous and broad-leaved mixed forests or temperate deciduous broad-leaved forests developed in the coastal areas of the North China Plain with scattered wetlands and swamps. The possible mechanism controlling this spatial heterogeneity of regional vegetation pattern in the North China Plain during the Middle Holocene is the warm and humid climate and sea level rise.

**Author Contributions:** M.X.: Conceptualization, Writing—Original Draft and Review, Visualization. Q.X.: Conceptualization, Writing—Review. Y.L.: Conceptualization, Writing—Review and Editing, Funding acquisition. T.D.: Conceptualization, Writing—Review. B.F.: Writing—Review and Editing. W.Z.: Writing—Review and Editing. B.L.: Conceptualization, Writing—Review and Editing, Funding acquisition. All authors have read and agreed to the published version of the manuscript.

**Funding:** This work was funded by National Natural Science Foundation of China Regional Innovation and Development Joint Fund (Grant No. U20A20116), National Natural Science Foundation of China (Grant No. 42271158), the Hebei Natural Science Foundation (Grant Nos. D2020205016, 18963301D), Hebei Normal University (Grant No. CXZZSS2022070), the State Scholarship Council (Grant No. CSC202008130001), State Key Laboratory of Loess and Quaternary Geology, Institute of Earth Environment, CAS under grant number SKLLOGZR2003 to Q.X.

**Institutional Review Board Statement:** Not applicable.

**Informed Consent Statement:** Not applicable.

**Data Availability Statement:** Not applicable.

**Acknowledgments:** We would like to thank the handling editor and reviewers for their constructive comments, which considerably improved this paper. Our gratitude is also extended to Shiyong Yu for improving the language.

**Conflicts of Interest:** The authors declare no conflict of interest.

## Appendix A

**Table A1.** Lithologic descriptions and photographs of three parallel drill cores (DG02, LD03 and LD04 cores) in the region.

DG02		LD03		LD04	
2–VIII (422–200 cm)	yellow-brown with a small quantity of gray-black sandy silt	3–IX (790–708 cm)	black peat layer	4–VIII (151–0 cm)	miscellaneous fill
2–VII (475–422 cm)	gray-black silt clay with a lot of organic matter			4–VII (261–151 cm)	light yellow-brown silt sand; silt clay with horizontal bedding
2–VI (706–475 cm)	light gray-green silt clay with a small quantity of silt sand laminates with wavy bedding and rust stains; the top 10 cm contains calcareous sedimentary nodules	3–VIII (875–790 cm)	green-gray clay	4–VI (467–261 cm)	olive-gray silt sand and silt clay with horizontal bedding and marine shell fragments at the bottom and a small quantity of rust in the upper part
		3–VII (880–875 cm)	black peat layer		
2–V (717–706 cm)	gray-black peat layer	3–VI (970–880 cm)	Light yellowish brown clay-chalky sand inter layer	4–V (567–467 cm)	light gray-green silt clay with a small quantity of thin silt sand layers, horizontal bedding and rust staining
2–IV (840–717 cm)	yellow-gray sandy silt with a small quantity of silt sand lenses	3–V (1300–970 cm)	black-gray clay–silt sand	4–IV (851–567 cm)	black-gray silt sand with a small quantity of thin clay layers, horizontal bedding and a small quantity of lacustrine and carbonized plants
2–III (1100–840 cm)	black-gray silt sand; Silt clay with multilevel bedding				
2–II (1105–1100 cm)	gray-black peat layer	3–IV (1318–1300 cm)	yellow-gray silt sand and silt clay	4–III (905–851 cm)	black-gray silt sand with a small quantity of thin clay layers, horizontal bedding and a small quantity of snail shell fragments
		3–III (1331–1318 cm)	gray-black silt sand containing snail shell fragments, and relatively high organic matter content	4–II (927–905 cm)	gray-black sandy silt containing carbonized plant residues
2–I (1200–1105 cm)	gray-white sandy silt, silt sand;	3–II (1345–1331 cm)	gray-white silt clay	4–I (1000–927 cm)	gray-white sandy silt containing a small quantity of weak calcareous deposits and organic matter
		3–I (1445–1345 cm)	gray-black; gray-green silt clay; silt sand		

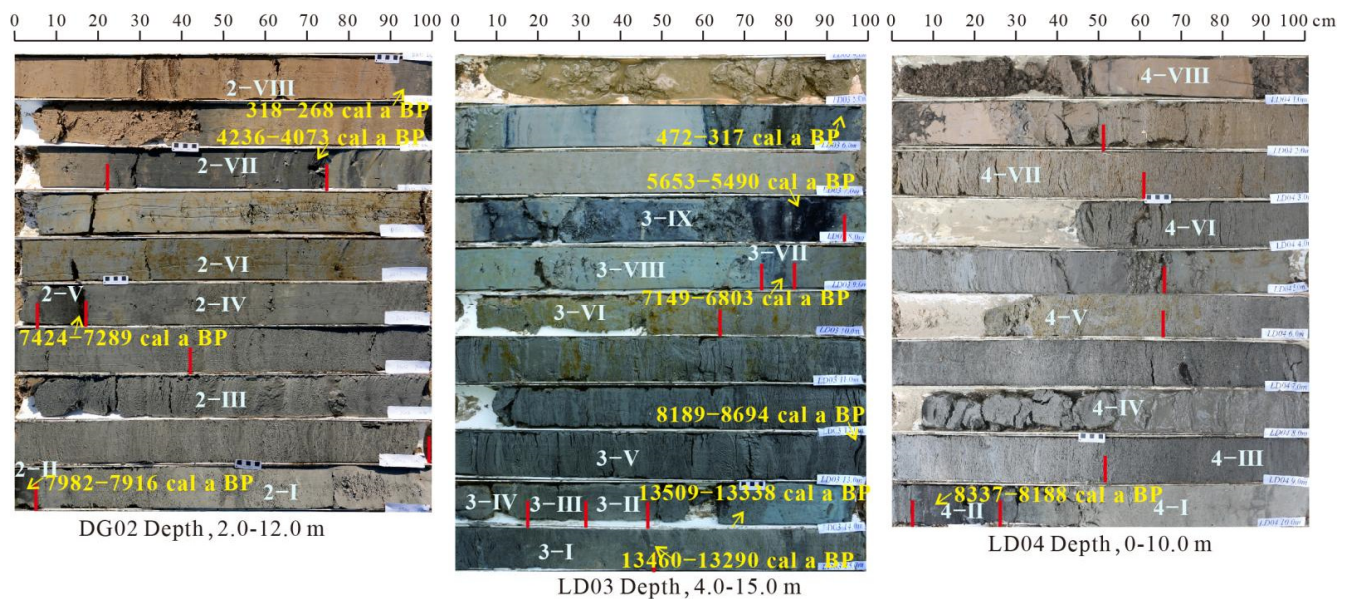


Figure A1. Image of cores DG02, LD03 and LD04 collected from the study area.

## References

- Xu, Q.H.; Zhang, S.R.; Gaillard, M.J.; Li, M.Y.; Cao, X.Y.; Tian, F.; Li, F.R. Studies of modern pollen assemblages for pollen dispersal-deposition-preservation process understanding and for pollen-based reconstructions of past vegetation, climate, and human impact: A review based on case studies in China. *Quat. Sci. Rev.* **2016**, *149*, 151–166. [\[CrossRef\]](#)
- Chen, W.Z.; Zhu, D.; Philippe, C.; Huang, C.J.; Nicolas, V.; Masa, K. Response of vegetation cover to CO<sub>2</sub> and climate changes between Last Glacial Maximum and pre-industrial period in a dynamic global vegetation model. *Quat. Sci. Rev.* **2019**, *218*, 293–305. [\[CrossRef\]](#)
- De Noblet Ducoudré, N.; Boisier, J.P.; Pitman, A.; Bonan, G.B.; Brovkin, V.; Cruz, F.; Delire, C.; Gayler, V.; van den Hurk, B.J.J.; Lawrence, P.J.M.; et al. Determining robust impacts of land-use-induced land cover changes on surface climate over North America and Eurasia: Results from the first set of LUCID experiments. *J. Clim.* **2012**, *25*, 3261–3281. [\[CrossRef\]](#)
- Gaillard, M.J.; Sugita, S.; Mazier, F.; Trondman, A.K.; Brostrom, A.; Hickler, T.; Kaplan, J.O.; Kjellstrom, E.; Kokfelt, U.; Kunes, P.; et al. Holocene land-cover reconstructions for studies on land cover-climate feedbacks. *Clim. Past* **2010**, *6*, 483–499. [\[CrossRef\]](#)
- Mayewski, P.A.; Rohling, E.E.; Stager, J.C.; Karlen, W.; Maasch, K.A.; Meeker, L.D.; Meyerson, E.A.; Gasse, F.; van Kreveld, S.; Holmgren, K.; et al. Holocene climate variability. *Quat. Res.* **2004**, *62*, 243–255. [\[CrossRef\]](#)
- Wang, S.M.; Wu, R.J.; Jiang, X.H. Environmental changes and paleoclimate since the last Glaciation in Daihai, Inner Mongolia. *Quat. Res.* **1990**, *3*, 223–232. (In Chinese)
- Chen, J.Y. Lichen chronology of Holocene glacial changes at the Headwaters of the Urumqi River in Tianshan Mountains. *Sci. China* **1988**, *1*, 95–104. (In Chinese)
- Xu, Q.H.; Li, Y.C.; Yang, X.L. Quantitative relationship between pollen and vegetation in northern China. *Earth Sci.* **2007**, *50*, 582–599. [\[CrossRef\]](#)
- Prentice, I.C.; Guiot, J.; Huntley, B.; Jolly, D.; Cheddadi, R. Reconstructing biomes from palaeoecological data: A general method and its implication to European pollen data at 0 and 6 ka. *Clim. Dynam.* **1996**, *12*, 185–194. [\[CrossRef\]](#)
- Tarasov, P.E.; Guiot, J.L.; Cheddadi, R.; Andreev, A.A.; Bezusko, L.G.; Blyakharchuk, T.A.; Dorofeyuk, N.I.; Filimonova, L.V.; Volkova, V.S.; Zernitskaya, V.P. Climate in northern Eurasia 6000 years ago reconstructed from pollen data. *Earth Planet Sci. Lett.* **1999**, *171*, 635–645. [\[CrossRef\]](#)
- Brostrom, A.; Gaillard, M.J.; Margaretha, I. Pollen-landscape relationships in modern analogues of ancient cultural landscapes in southern Sweden—a first step towards quantification of vegetation openness in the past. *Veg. Hist. Archaeobotany* **1998**, *7*, 189–201. [\[CrossRef\]](#)
- Zheng, Y.W.; Zheng, Z.; Huang, K.Y.; Pan, A.D.; Ma, H.Z.; Wei, J.H.; Wei, H.C. Qaidam Basin 6.0 ka B.P., 2.5 ka B.P. and modern vegetation coverage reconstruction. *Quat. Sci.* **2009**, *29*, 701–710.
- Nielsen, A.B.; Odgaard, B.V. The use of historical analogues for interpreting fossil pollen records. *Veg. Hist. Archaeobotany* **2004**, *13*, 33–43. [\[CrossRef\]](#)
- Sugita, S. Theory of quantitative reconstruction of vegetation I: Pollen from large sites REVEALS regional vegetation composition. *Holocene* **2007**, *17*, 229–241. [\[CrossRef\]](#)
- Bunting, M.J.; Armitage, R.; Binney, H.A. Estimates of relative pollen productivity and relevant source area of pollen for major tree taxa in two Norfolk(UK) woodlands. *Holocene* **2005**, *15*, 459–465. [\[CrossRef\]](#)

16. Trondman, A.K.; Gaillard, M.J.; Mazier, F.; Sugita, S.; Fyfe, R.; Nielsen, A.B.; Twiddle, C.; Barratt, P.; Birks, H.J.B.; Bjune, A.E. Pollen-based quantitative reconstructions of Holocene regional vegetation cover (plant-functional types and land-cover types) in Europe suitable for climate modeling. *Glob. Chang. Biol.* **2015**, *21*, 676–697. [[CrossRef](#)]
17. Xu, Q.H.; Cao, X.Y.; Tian, F.; Zhang, S.R.; Li, Y.C.; Li, M.Y.; Li, J.; Liu, Y.L.; Liang, J. Pollen productivity in the typical grassland area of northern China and its role in quantitative reconstruction of paleovegetation. *China Earth Sci.* **2013**, *43*, 2016–2028.
18. Wang, Y.B.; Herzschuh, U. Reassessment of Holocene vegetation change on the upper Tibetan Plateau using the pollen-based REVEALS model. *Rev. Palaeobot. Palynol.* **2011**, *168*, 31–40. [[CrossRef](#)]
19. Li, F.R.; Gaillard, M.J.; Xu, Q.H.; Bunting, M.J.; Li, Y.C.; Li, J.; Mu, H.S.; Lu, J.Y.; Zhang, P.P.; Zhang, S.R.; et al. Review of relative pollen productivity estimates from temperate China for pollen-based quantitative reconstruction of past plant cover. *Front. Plant Sci.* **2018**, *9*, 1214. [[CrossRef](#)]
20. Ni, J. Palynological biota regionalization and quantitative reconstruction of paleovegetation. *Quat. Res.* **2013**, *33*, 1091–1100. (In Chinese)
21. Liu, L. *Hebei Vegetation*; Science Press: Beijing, China, 1996; pp. 268–273. (In Chinese)
22. Peng, Y.J.; Xiao, J.; Nakamura, T.; Liu, B.L.; Inouchi, Y. Holocene East Asian monsoonal precipitation pattern revealed by grain-size distribution of core sediments of Daihai Lake in Inner Mongolia of north-central China. *Earth Planet. Sci. Lett.* **2005**, *223*, 467–479. [[CrossRef](#)]
23. Rao, Z.G.; Jia, G.D.; Li, Y.X.; Chen, J.H.; Xu, Q.H.; Chen, F.H. Asynchronous evolution of the isotopic composition and amount of precipitation in north China during the Holocene revealed by a record of compound-specific carbon and hydrogen isotopes of long-chain n-alkanes from an alpine lake. *Earth Planet. Sci. Lett.* **2016**, *446*, 68–76. [[CrossRef](#)]
24. Chen, F.H.; Wu, D.; Chen, J.H.; Zhou, A.F.; Yu, J.Q.; Shen, J.; Wang, S.M.; Huang, X.Z. Holocene moisture and East Asian summer monsoon evolution in the northeastern Tibetan Plateau recorded by Lake Qinghai and its environs: A review of conflicting proxies. *Quat. Sci. Rev.* **2016**, *154*, 111–129. [[CrossRef](#)]
25. Liu, X.X.; Vandenberghe, J.; An, Z.S.; Li, Y.; Jin, Z.D.; Dong, J.B.; Sun, Y.B. Grain size of Lake Qinghai sediments: Implications for riverine input and Holocene monsoon variability. *Palaeogeogr. Palaeoclimatol. Palaeoecol.* **2016**, *449*, 41–51. [[CrossRef](#)]
26. Tong, G.B.; Ke, M.H.; Yu, S.F. Quaternary palynological assemblages in Hebei Plain and their geological significance. *Mar. Geol. Quat. Geol.* **1983**, *04*, 91–103. (In Chinese)
27. Yu, G.; Sun, X.J.; Qin, B.Q.; Song, C.Q.; Li, H.Y.; Prentice, L.C.; Harrison, S.P. Mid-holocene vegetation distribution in China simulated by pollen vegetations. *Earth Sci.* **1998**, *01*, 73–78.
28. Chen, Y.; Ni, J. Quantitative reconstruction of large-scale paleovegetation patterns using palynological records. *J. Plant Ecol.* **2008**, *05*, 1201–1212. (In Chinese)
29. Tian, F.; Cao, X.Y.; Dallmeyer, A.; Ni, J.; Zhao, Y.; Wang, Y.B. Quantitative woody cover reconstructions from eastern continental Asia of the last 22 kyr reveal strong regional peculiarities. *Quat. Sci. Rev.* **2016**, *137*, 33–44. [[CrossRef](#)]
30. Wu, C. *Evolution of the Natural Environment of the North China Plain in the Last 40,000 Years*; China Science and Technology Press: Beijing, China, 1992. (In Chinese)
31. Qin, X.G.; Liu, D.S.; Cai, B.K.; Lu, H.Y. Environmental patterns and vegetation succession zones of typical time periods in northern China and their implications for ecological environment construction. *Sci. Soil Water Conserv. China* **2003**, *2*, 1–7. (In Chinese)
32. Shi, Y.F.; Kong, Z.C.; Wang, S.M.; Tang, L.Y.; Wang, F.B.; Yao, C.D.; Zhao, X.T.; Zhang, P.Y.; Shi, S.H. Climate fluctuations and important events during the Holocene warm period in China. *Sci. China* **1992**, *12*, 1300–1308. (In Chinese)
33. Ren, G.P. Background vegetation of northern China. *Acta Ecol. Sin.* **2004**, *6*, 1287–1293. (In Chinese)
34. Xu, Q.H.; Chen, S.Y.; Kong, Z.C.; Du, N.Q. Preliminary study on vegetation succession and climate change since Holocene in Baiyangdian Area. *J. Plant Ecol. Bot.* **1988**, *2*, 65–73. (In Chinese)
35. Xiao, J.Y.; Chen, J.Q.; Xu, Z.P.; Cao, G.C.; Zhao, Q.L.; Gao, L.W. Characteristics of vegetation fluctuation and its response to climate change since Late Pleistocene in Handan Area. *J. Sediment.* **2010**, *28*, 1206–1212. (In Chinese)
36. Zhang, W.Q. Late Pleistocene palynological assemblages and their paleo-environmental evolution in Ningjinpo. *J. Micropalaeontology* **1999**, *4*, 431–438. (In Chinese)
37. Cao, X.Y.; Xu, Q.H.; Jing, Z.C.; Tang, J.G.; Li, Y.C.; Tian, F. Holocene climate change and human impacts implied from the pollen records in Anyang, central China. *Quat. Int.* **2010**, *227*, 3–9. [[CrossRef](#)]
38. Sun, Y.H. *Pollen-Based Quantitative Vegetation-Cover Reconstruction for Northern China during the Last 6000 Years*; Hebei Normal University: Shijiazhuang, China, 2020.
39. Weltje, G.J.; Prins, M.A. Genetically meaningful decomposition of grain-size distributions. *Sediment. Geol.* **2007**, *202*, 409–424. [[CrossRef](#)]
40. Paterson, G.A.; Heslop, D. New methods for unmixing sediment grain size data. *Geochemistry* **2015**, *16*, 4494–4506. [[CrossRef](#)]
41. Sun, D.H.; An, Z.S.; Su, R.X. The mathematical approach for separating of sedimentary components and its applications in palaeoenvironment. *Prog. Nat. Sci.* **2001**, *11*, 47–54.
42. Nottebaum, V.; Stauch, G.; Hartmann, K. Unmixed loess grain size populations along the northern Qilian Shan (China): Relationships between geomorphologic, sedimentologic and climatic controls. *Quat. Int.* **2015**, *372*, 151–166. [[CrossRef](#)]
43. Yu, S.Y.; Colman, S.M.; Li, L.X. BEMMA: A hierarchical Bayesian End-member modeling analysis of sediment grain-size distributions. *Math. Geosci.* **2016**, *48*, 723–741. [[CrossRef](#)]
44. Dietze, E.; Dietze, M. Grain-size distribution unmixing using the R package EMMAgeo. *EG Quat. Sci. J.* **2019**, *68*, 29–46. [[CrossRef](#)]

45. Li, J.Q.; Li, X.Q.; Fan, B.S.; Wang, Z.X.; Li, Y.C.; Liu, L.J.; Hou, X.W.; Zhang, C.C. Environmental changes during the Middle Pleistocene climate transition in Changzhi Basin, Shanxi Province. *J. Geol.* **2021**, *95*, 3532–3543. (In Chinese)
46. Faegri, K.; Kaland, P.E.; Krzywinski, K. Textbook of pollen analysis. *J. Biogeogr.* **1998**, *12*, 238.
47. Ran, J.; Du, G.; Pan, Z.X. Comparison of methods for grain size analysis of sediments. *Rock Miner. Anal.* **2011**, *30*, 669–676. (In Chinese)
48. Liu, X.M.; Luo, W. Application of particle size analysis in sediment research. *Exp. Technol. Manag.* **2013**, *30*, 20–23. (In Chinese)
49. Zhang, Y.; Wei, Q.; Zhang, Z.; Xu, Q.H.; Gao, W.M.; Li, Y.C. Relative pollen productivity estimates of major plant taxa and relevant source area of pollen in the warm-temperate forest landscape of northern China. *Veg. Hist. Archaeobotany* **2021**, *30*, 231–241. [[CrossRef](#)]
50. Li, M.Y.; Zhang, S.R.; Xu, Q.H.; Xiao, J.L.; Wen, R.L. Spatial patterns of vegetation and climate in the North China Plain during the Last Glacial Maximum and Holocene climatic optimum. *Earth Sci.* **2019**, *62*, 1279–1287. [[CrossRef](#)]
51. Zhao, L.; Ma, C.; Xu, Q.M.; Deng, Y.K.; Shang, G.C.; Tang, L.Y. Vegetation evolution in response to climate change and rapid sea-level rise during 8.2–7.0 cal ka BP: Pollen evidence from the northwest coast of Bohai Bay, north China. *Catena* **2021**, *196*, e104869. [[CrossRef](#)]
52. Sun, Y.H.; Xu, Q.H.; Zhang, S.R. Pollen-based temporal-spatial land cover reconstruction in North China for the last 6000 years. *Quat. Int.* **2022**, *641*, 6–14. [[CrossRef](#)]
53. Wang, H.; Li, F.L.; Fan, C.F.; Frechen, M.; Strydonck, M.; Pei, Y.D.; Wang, Y.S. The <sup>14</sup>C dataset of the coastal zone around the Bohai Sea (I). *Quat. Res.* **2004**, *6*, 601–603. (In Chinese)
54. Wang, H.; Fan, C.F. The <sup>14</sup>C dataset of the coastal zone around the Bohai Sea (II). *Quat. Res.* **2005**, *2*, 141–156. (In Chinese)
55. Li, Y.G.; Wei, F.; Zhou, L.P. Determination of AMS <sup>14</sup>C age of peat samples: Whole sample, plant residue and sporopollen concentrate. *Quat. Res.* **2007**, *4*, 499–506. (In Chinese)
56. Reamer, P.J.; Bard, E.; Bayliss, A.; Beck, J.W.; Blackwell, P.G.; Ramsey, C.B.; Buck, C.E.; Cheng, H.; Edwards, R.L.; Friedrich, M.; et al. IntCal13 and Marine13 radiocarbon age calibration curves 0–50,000 years cal BP. *Radiocarbon* **2013**, *55*, 1869–1887. [[CrossRef](#)]
57. Liu, X.; Zhang, Y.Z.; Xia, F.; Wang, R.; Ren, S.; WüNNEMANN Bernd. Holocene sedimentary environment evolution in Lunden Bay, southern North Sea. *Geogr. Res.* **2017**, *36*, 2261–2276. (In Chinese)
58. Ferguson, S.; Warny, S.; Anderson, J.B.; Simms, A.R.; Escarguel, G. Holocene vegetation and climate evolution of corpus christi and trinity bays: Implications on coastal texas source-to-sink deposition. *Geobios* **2018**, *51*, 123–135. [[CrossRef](#)]
59. Razjigaeva, N.G.; Grebennikova, T.A.; Ganzey, L.A.; Mokhova, L.M.; Bazarova, V.B. The role of global and local factors in determining the middle to late Holocene environmental history of the South Kurile and Komandar islands, northwestern Pacific. *Palaeogeogr. Palaeoclimatol. Palaeoecol.* **2004**, *209*, 313–333. [[CrossRef](#)]
60. Wang, X.M.; Sun, X.J.; Wang, P.X.; Statterger, K. Sporulation and algae of the Sunda shelf since the last ice age and their palaeoenvironmental significance. *J. Paleontol.* **2008**, *03*, 313–318.
61. Alizadeh, K.; Cohen, M.; Behling, H. Origin and dynamics of the northern South American coastal savanna belt during the Holocene—the role of climate, sea-level, fire and humans. *Quat. Sci. Rev.* **2015**, *122*, 51–62. [[CrossRef](#)]
62. Zhuang, Z.Y.; Xu, W.D.; Li, X.L. Shoreline evolution of the southern coast of the Bohai Sea in the past 6000 years. *J. Ocean. Univ. Qingdao* **1991**, *02*, 99–110. (In Chinese)
63. An, Z.S.; Colman, S.M.; Zhou, W.J.; Li, X.Q.; Brown, E.T.; Jull, A.J.T.; Cai, Y.J.; Huang, Y.S.; Lu, X.F.; Chang, H.; et al. Interplay between the Westerlies and Asian monsoon recorded in Lake Qinghai sediments since 32 ka. *Sci. Rep.* **2012**, *2*, 619. [[CrossRef](#)]
64. Lu, F.Z.; Ma, C.M.; Zhu, C.; Lu, H.Y.; Zhang, X.J.; Huang, K.Y.; Guo, T.H.; Li, K.F.; Li, L.; Li, B.; et al. Variability of East Asian summer monsoon precipitation during the Holocene and possible forcing mechanisms. *Clim. Dyn.* **2019**, *52*, 969–989. [[CrossRef](#)]
65. Pisaric, M.F.J.; Szeicz, J.M.; Karst, T.; Smol, J.P. Comparison of pollen and conifer stomates as indicators of alpine tree line in northwestern Canadian lake sediments. *Can. J. Bot.* **2000**, *78*, 1180–1186.
66. Wan, H.W.; Shen, J.; Tang, L.Y.; Li, C.H. Stomatal apparatus morphology of Pinaceae and Cupressaceae in Northwest China. *J. Micropalaeontology* **2007**, *24*, 309–319. (In Chinese)
67. Hansen, B.C.S. Conifer stomate analysis as a paleoecological tool: An example from the Hudson Bay Lowlands. *Can. J. Bot.* **1995**, *73*, 244–252. [[CrossRef](#)]
68. Finsinger, R.W.; Tinne, R.W. Pollen and plant macrofossils at Lac de Fully (2135 m a.s.l.): Holocene forest dynamics on a highland plateau in the Valais, Switzerland. *Holocene* **2007**, *17*, 1119–1127. [[CrossRef](#)]
69. Chen, F.H.; Xu, Q.H.; Chen, J.H.; Birks, H.B.; Liu, J.B.; Zhang, S.R.; Jin, L.Y.; An, C.B.; Telford, J.; Cao, X.Y.; et al. East Asian summer monsoon precipitation variability since the last deglaciation. *Sci. Rep.* **2015**, *5*, 11186. [[CrossRef](#)] [[PubMed](#)]
70. Jiang, M.; Han, Z.; Li, X.; Wang, Y.; Stevens, T.; Cheng, J.; Lu, C.; Zhou, Y.; Yang, Q.; Xu, Z. Beach ridges of Dali Lake in Inner Mongolia reveal precipitation variation during the Holocene. *Quaternary Sci.* **2020**, *35*, 716–725. [[CrossRef](#)]
71. Huang, C.; Lai, Z.P.; Liu, X.J.; David, M. Lake-level history of Qinghai Lake on the NE Tibetan Plateau and its implications for Asian monsoon pattern—A review. *Quat. Sci. Rev.* **2021**, *273*, 107258. [[CrossRef](#)]
72. Li, G.Q.; Wang, Z.; Zhao, W.W.; Jin, M.; Wang, X.Y.; Tao, S.X.; Chen, C.Z.; Cao, X.Y.; Zhang, Y.N.; Yang, H. Quantitative precipitation reconstructions from Chagan Nur revealed lag response of East Asian summer monsoon precipitation to summer insolation during the Holocene in arid northern China. *Quat. Sci. Rev.* **2020**, *239*, 106365. [[CrossRef](#)]

73. Dong, J.G.; Shen, C.C.; Kong, X.G.; Wang, H.C.; Jiang, X.Y. Reconciliation of hydroclimate sequences from the Chinese Loess Plateau and low-latitude East Asian Summer Monsoon regions over the past 14,500 years. *Palaeogeogr. Palaeoclimatol. Palaeoecol.* **2015**, *435*, 127–135. [[CrossRef](#)]
74. Li, B.; Ma, C.M.; Zhu, C.; Li, K.F.; Zhu, X.H.; Tan, Y.; Wang, K.H.; Guo, T.H.; Jia, T.J. Stratigraphic record of holocene environmental evolution in pingwangkong, eastern taihu plain. *Acta Palaeontol. Sin.* **2018**, *57*, 513–523. (In Chinese)
75. Wang, S.M.; Yang, X.D.; Ma, Y.; Pan, H.X.; Tong, G.B.; Wu, X.H. Study on the relationship between environmental changes and paleo-monsoon in gucheng lake, jiangsu province since 15ka. *Sci. China* **1996**, *2*, 137–141. (In Chinese)
76. He, K.Y.; Lu, H.Y.; Zheng, Y.F.; Zhang, J.P.; Xu, D.K.; Huan, X.J.; Wang, J.H.; Lei, S. Middle-Holocene sea-level fluctuations interrupted the developing Hemudu culture in the lower Yangtze River, China. *Quat. Sci. Rev.* **2018**, *188*, 90–103. [[CrossRef](#)]
77. Xu, Q.H.; Yang, X.L.; Wang, Z.H.; Wu, C.; Meng, L.Y.; Yao, Z.J. A preliminary study on river transport of pollen. *Bot. Gaz.* **1995**, *10*, 829–832. (In Chinese)
78. Pang, R.M.; Xu, Q.H.; Ding, W.; Zhang, S.R. Characteristics of agricultural palynological assemblages in central and southern Hebei Province. *J. Geogr.* **2010**, *65*, 1345–1354. (In Chinese)
79. Zhao, Y.; Yu, Z.C. Vegetation response to Holocene climate change in East Asian monsoon-margin region. *Earth-Sci. Rev.* **2012**, *113*, 1–10. [[CrossRef](#)]
80. Gupta, A. Assessment of Quaternary Vegetation and Climate of Kumaun Himalaya (Saria Tal)-Geochemical Analysis. *Vegetos* **2010**, *23*, 55–67.
81. Wen, R.L.; Xiao, J.L.; Chang, Z.; Zhai, D.; Xu, Q.H.; Li, Y.C.; Itoh, S. Holocene precipitation and temperature variations in the East Asian monsoonal margin from pollen data from Hulun Lake in northeastern Inner Mongolia, China. *Boreas* **2010**, *39*, 262–272. [[CrossRef](#)]
82. Xiao, J.L.; Xu, Q.H.; Nakamura, T.; Yang, X.; Liang, W.; Inouchi, Y. Holocene vegetation variation in the Daihai Lake region of north-central China: A direct indication of the Asian monsoon climatic history. *Quat. Sci. Rev.* **2004**, *23*, 1669–1679. [[CrossRef](#)]